RSC Advances

PAPER

View Article Online
View Journal | View Issue

Cite this: *RSC Adv.*, 2025, **15**, 36710

Development of a polyvinyl alcohol-capped copper nanocluster-integrated electrochemical sensor for trace-level monitoring of anthraquinone

Saba A. Memon,[a] Huma Shaikh,[a] Jamil A. Buledi,[a] Amber R. Solangi,*[a] Saima Q. Memon[b] and Tania Ghumro[c]

In the current study, polyvinyl alcohol-capped copper nanoclusters (PVA-CuNCs) were synthesized *via* a chemical reduction method using PVA as a capping and stabilizing agent. The synthesized PVA-CuNCs were used for the fabrication of an ultra-sensitive electrochemical sensor to detect anthraquinone (AQ) at trace levels in an aqueous environment. The fabricated nanoclusters were thoroughly characterized using a wide range of analytical tools. FTIR analysis confirmed the functional properties of the PVA-CuNCs, while XRD investigation revealed a crystalline nature with an average size of 4.21 nm. Their elemental composition was assessed through EDX, indicating a clean copper-based matrix without any notable impurity. Furthermore, the DLS showed an average hydrodynamic diameter of 2.71 nm, and AFM imaging provided a 2D/3D surface profile with a particle size of approximately 6.5 nm. The synthesized nanocluster was then immobilized on a platinum electrode to fabricate a PVA-CuNCs/PtE sensor, which was employed for the electrochemical detection of AQ. Under optimized conditions, such as phosphate-buffered saline at pH 6, a scan rate of 220 mV s^{-1}, and a potential window of −0.4 to +0.8 V, the sensor demonstrated a sensitive and linear response to AQ, with an LOD of 0.056 μM and an LOQ of 0.17 μM. The fabricated sensor also performed exceptionally well in real water samples, including river water and industrial wastewater, showing recovery values within acceptable limits. The results confirm the potential of PVA-CuNCs as an efficient and reliable sensing platform for AQ detection in environmental monitoring.

Received 18th August 2025
Accepted 18th September 2025

DOI: 10.1039/d5ra06099k

rsc.li/rsc-advances

1 Introduction

Quinone compounds are a class of aromatic organic molecules characterized by a fully conjugated cyclic dione structure, typically derived from aromatic compounds by replacing two hydrogen atoms with two oxygen atoms in the form of carbonyl groups (C=O).[1,2] Anthraquinone, alternatively known as anthracenediones or dioxoanthracenes, holds a significant position within the quinone family.[3,4] This group includes a considerable arrangement of structurally diverse compounds that belong to the polyketide class.[5] Essentially, anthraquinone is an aromatic organic molecule. Moreover, anthraquinone-based compounds are widely used in various industrial products such as dyes, cosmetics, textiles, chemicals, pharmaceuticals and electroplating industries.[6,7] Beyond their applications in those sectors, anthraquinone derivatives are also used in numerous cosmetic products. These substances can readily permeate the human body through the skin and respiratory pathways.[8] Their limited biodegradability, potential to damage genetic material (genotoxicity), capacity to induce cancer (carcinogenicity), and overall toxic effects raise concerns about various health disorders.[9,10] However, the widespread presence of anthraquinone in the ecological system has led both the United States Environmental Protection Agency (US EPA) and the European Union (EU) to classify it as a priority environmental pollutant. This label reflects the significant concerns associated with its persistence and potential harm to the environment and human health.[11,12] Consequently, the identification and measurement of these quinone substances within biological systems are of vital importance for monitoring environmental quality and advancing industrial research endeavors.

To date, a variety of methodologies have been developed for the detection and quantification of anthraquinone-based compounds in the wastewater system. These include techniques such as spectrophotometry, fluorescence spectroscopy, chemiluminescence, solid-phase extraction, and various chromatographic methods.[13–15] Nevertheless, the majority of these established techniques present certain limitations. These drawbacks encompass high operational costs, lengthy analysis times, the necessity for complex and specialized

[a]*National Centre of Excellence in Analytical Chemistry, University of Sindh, Jamshoro 76080, Pakistan. E-mail: amber.solangi@usindh.edu.pk*

[b]*M. A. Kazi Institute of Chemistry, University of Sindh, Jamshoro 76080, Pakistan*

[c]*Department of Human and Rehabilitation Science, Begum Nusrat Bhutto Women University, Sukkur, Pakistan*

instrumentation, and limited sensitivity in detecting low concentrations. In contrast to these approaches, electrochemical detection methods for anthraquinone-based compounds have gained considerable interest due to their operational simplicity, enhanced sensitivity, cost-effectiveness, high catalytic efficiency, and minimal analysis time.[16–20] However, a notable limitation of electrochemical methods lies in the potential for overlapping electrochemical signals when analyzing mixtures of structurally similar phenolic compounds. Therefore, to address these challenges, the development of novel electrocatalysts exhibiting improved sensitivity and selectivity for the detection of anthraquinone compounds stands as a significant demand within the field of electrochemistry. In this connection, metal nanoclusters (MNCs) represent a fascinating and adaptable class of nanomaterials, exhibiting characteristics that bridge the gap between individual metal atoms and larger metal nanoparticles (MNPs). The MNCs have been a choice of interest in electrochemical detection to enhance sensitivity, selectivity and stability of chemically modified sensors. The current sensing methodologies employing MNCs predominantly utilize noble metals, like silver and gold nanoclusters, being prominent examples.[21] Meanwhile, copper nanoclusters (CuNCs) have been increasingly attracting attention. This growing interest stems from their chemical similarities to silver (AgNCs) and gold (AuNCs), their distinctive fluorescent properties, and significantly, the economic advantages and easy accessibility of their precursor materials, along with relatively simple synthesis procedures.[22–24] Furthermore, a variety of techniques have been utilized to synthesize CuNCs with precise atomic control. These methods include photoreduction, solvothermal synthesis, chemical reduction, ultrasound-assisted synthesis, microwave irradiation, and chemical etching. These diverse approaches have facilitated the production of CuNCs for innovative applications within the field of analytical chemistry.[25–28] In addition, various ligand systems have been introduced to enhance the optical properties and quantum yield of synthesized CuNCs. Considerable efforts have been made toward the production of CuNCs through the utilization of diverse organic molecules. These molecules include oligonucleotides, peptides, curcuma root, and proteins.[29,30] Amongst them, polyvinyl alcohol (PVA) is a widely used capping agent in the synthesis of nanomaterials. PVA is a water-soluble polymer with a high molecular weight that can form a stable coating around the nanomaterials. The role of PVA as a capping agent in the synthesis of nanomaterials includes stabilization, control of particle size and shape, reduction of toxicity and enhanced dispersibility.[31,32]

In the current experiment, the PVA-CuNCs were fabricated through a chemical reduction method and were employed as a sensitive and selective sensing material for the determination of anthraquinone from wastewater samples.

2 Experimental

2.1 Chemicals and solution

All the chemicals used in the current experiments were highly pure and used without any further purification. Copper chloride ($CuCl_2$), anthraquinone (AQ), sodium borohydride ($NaBH_4$) and polyvinyl alcohol were purchased from Merck, Germany. Ascorbic acid, pentachlorophenol (PCP), trichlorophenol (TCP), hydroquinone (HQ), benzoquinone (BQ), and hydrobromic acid (HBA) were obtained from Sigma-Aldrich, Germany. A 0.1 M phosphate-buffered saline (PBS) at pH 6 was used for the electrochemical oxidation of anthraquinone. The pH of the electrolyte was adjusted using 0.1 M NaOH and 0.1 M HCl.

2.2 Instrumentation

To confirm the successful synthesis and evaluate the structural, morphological, elemental and electrochemical properties of PVA-CuNCs, several characterization methods were employed. The presence of functional groups was analyzed using Fourier transform infrared (FTIR) spectroscopy (Thermo Nicolet 5700) which provided insight into the chemical bonding and surface functionalities of the NCs. The X-ray diffraction analysis was carried out to investigate the crystalline nature and average crystallite size of PVA-CuNCs using an X-ray diffractometer (Model XRD-7000, Shimadzu Scientific Instruments). The average size of dispersed PVA-CuNCs was calculated through dynamic light scattering (DLS) model (Zetasizer Nano-ZS ZEN 3600). The 3D surface morphology and size of the fabricated material were investigated *via* an atomic force microscope (AFM) (Model 550, Agilent, Santa Clara, CA, USA).

The electrochemical detection of AQ was performed using a CHI-760 electrochemical workstation, USA. In a standard three-electrode configuration, the PVA-CuNC-modified platinum electrode (PtE) served as the working electrode, with a platinum wire as the counter electrode and Ag/AgCl as the reference electrode.

2.3 Synthesis of polyvinyl alcohol/copper nanoclusters (PVA-CuNCs)

For the synthesis of PVP/CuNCs, 10 mM of copper chloride ($CuCl_2 \cdot H_2O$) solution was prepared in 10 mL of deionized (DI) water, followed by the preparation of 100 mM fresh $NaBH_4$ solution in 15 mL of DI water. For capping, 16.6 mM polyvinyl alcohol (PVA) was prepared in 20 mL of DI water. At first, 500 μL of PVA and 1 mL of $NaBH_4$ were mixed in 25 mL of DI water and stirred at 1200 rpm for 20 minutes. Then, 4 mL of copper chloride (10 mM) was added dropwise to the above solution, and the color of the solution changed from dark-brown to light yellow with the evolution of H_2 gas. After the gas has settled, another 1 mL of $NaBH_4$ was added to the above solution with constant stirring at 1200 rpm for 4 h. At this stage, the PVA-CuNCs were successfully synthesized. After successful synthesis, the PVA-CuNCs were washed with DI water and centrifuged at 4000 rpm to remove residual impurities from the final product.

2.4 Fabrication of PVA-CuNC/PtE

To modify a bare platinum electrode (PtE), a technique known as drop casting was employed,[33,34] utilizing polyvinyl alcohol copper nanoclusters (PVA-CuNCs). The modified electrode was prepared by first suspending 3 mg of the synthesized PVA-

CuNCs in 3 mL of deionized (DI) water. Subsequently, 40 μL of Nafion solution was introduced into this suspension, which acted as a binder. The resulting mixture of PVA-CuNCs and Nafion was then subjected to ultrasonication for 20 minutes to ensure the creation of a homogenous dispersion. The surface of the PtE was polished using an aluminum slurry with a pore size of 0.5 micrometers (μm). Following this polishing step, the PtE surface was rinsed thoroughly with DI water and further cleaned by ultrasonication in 30 mL of ethanol solution for 20 minutes. After the cleaning procedure, a 5 μL aliquot of the prepared PVA-CuNCs suspension was carefully applied onto the PtE's surface. The modified electrode was then dried at ambient temperature for 20 minutes, allowing the PVA-CuNC material to firmly attach to the electrode surface. Upon successful deposition, the resulting electrode was designated as the PVA-CuNCs/PtE.

3 Results and discussion

3.1 FTIR and XRD investigation of PVA-CuNCs

Fourier-transform infrared spectroscopy (FTIR) was used to investigate the chemical structure and functional groups present in the PVA-capped copper nanoclusters (PVA-CuNCs), as displayed in Fig. 1(a). The broad absorption band observed around 3415 cm^{-1} is attributed to the O–H stretching vibrations, which indicate the presence of polyvinyl alcohol molecules. A distinct signal at 2966 cm^{-1} is assigned to the C–H stretching of alkyl groups, suggesting the involvement of polyvinyl alcohol (PVA) in the surface capping. The C=C stretching vibration was evident from the band appearing near 1651 cm^{-1}, which may be associated with minor unsaturated bonds introduced during the synthesis. The $-CH_2$ bending mode was confirmed by the peak at 1424 cm^{-1}. Furthermore, the C–O stretching was identified at 1290 cm^{-1}, verifying the presence of alcohol or ether functionalities from the PVA chains. A well-defined band at 1013 cm^{-1} corresponds to the C–H bending from PVA chains. Notably, the characteristic peaks at 533 cm^{-1} and 559 cm^{-1} are assigned to the symmetric and asymmetric stretching vibrations of Cu–Cu bonds, confirming the successful formation of copper nanoclusters. Moreover, X-ray diffraction (XRD) analysis was conducted to examine the crystalline nature and phase purity of the synthesized PVA-CuNCs, and the patterns are shown in Fig. 1(b). The diffraction pattern displayed prominent peaks corresponding to the crystal planes (111), (200), and (220). These reflections match well with the face-centered cubic (fcc) structure of metallic copper, indicating the high crystallinity of the nanoclusters. No secondary or impurity phases were detected, confirming the phase purity of the sample. Using the Debye–Scherrer formula, the average crystallite size of the PVA-CuNCs was estimated to be approximately 4.82 nm, reflecting the nanoscale dimensions of the synthesized clusters. The FTIR and XRD investigation confirmed the successful synthesis of PVA-CuNCs.

3.2 Elemental composition and size determination of PVA-CuNCs

Energy-dispersive X-ray spectroscopy (EDX) was employed to determine the elemental composition of the prepared PVA-capped copper nanoclusters. The spectrum revealed the presence of three key elements: carbon (C), oxygen (O), and copper (Cu), with their respective atomic percentages recorded as 23.42%, 36.41%, and 40.17%, as shown in Fig. 2(a). The significant carbon content reflects the contribution from the PVA matrix, which acts as a stabilizing and capping agent during the formation of copper nanoclusters. The oxygen component is primarily attributed to the hydroxyl groups present in PVA, as well as possibly surface-adsorbed water or slight oxidation of the copper surfaces. The relatively high percentage of copper confirms the successful formation and high yield of the nanoclusters, forming the core structure of the material. These results provide clear evidence that the

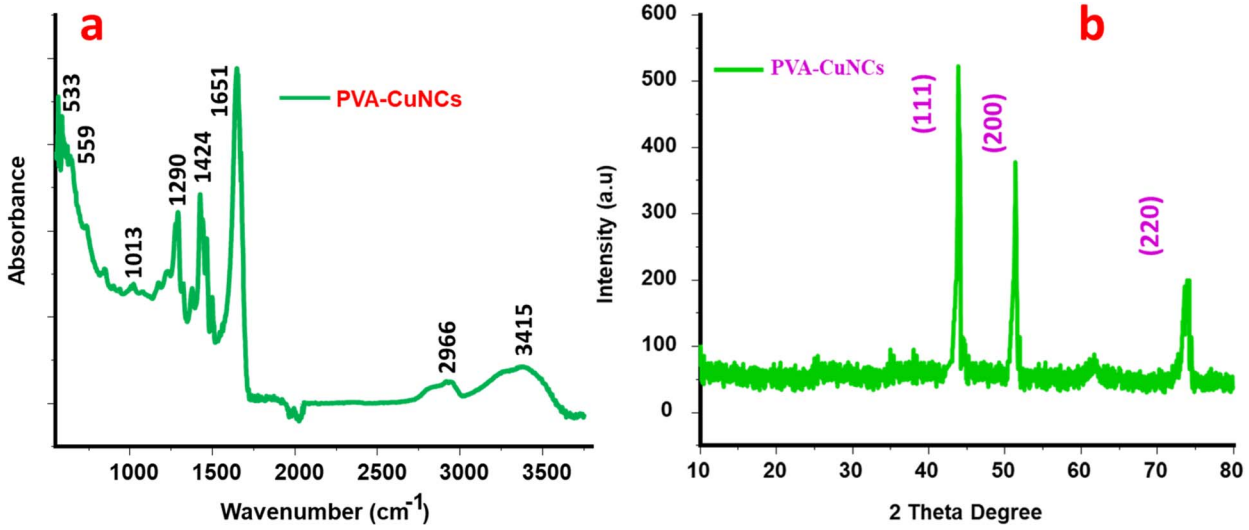

Fig. 1 (a) FTIR analysis of PVA-CuNCs confirming their surface functionalities and (b) XRD patterns of PVA-CuNCs displaying their crystalline structure.

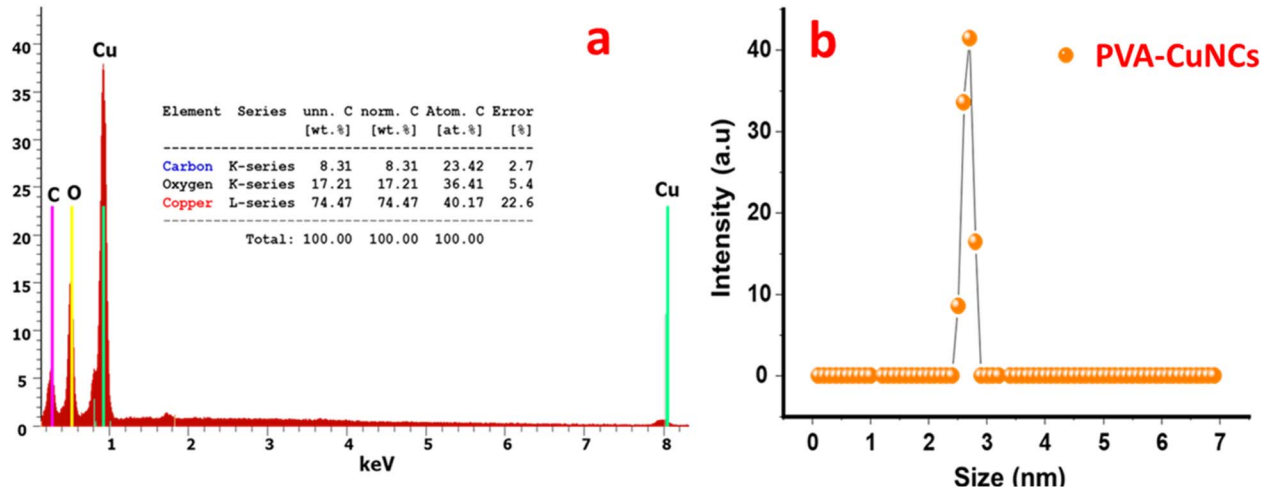

Fig. 2 (a) EDX analysis of the elemental composition of PVA-CuNCs and (b) DLS analysis for the size determination of PVA-CuNCs.

synthesized material consists of copper nanoclusters effectively stabilized within the organic polymeric framework. Moreover, the DLS measurement was carried out using a Zetasizer to evaluate the hydrodynamic diameter of the synthesized PVA-CuNCs. The particle size distribution curve, as illustrated in Fig. 2(b), showed that the average particle size was approximately 2.71 nm, indicating a narrow and uniform size distribution. The small particle size is a strong indication of successful nanocluster formation at the atomic or near-atomic level. This is consistent with the expected behavior of Cu nanoclusters capped with a polymeric stabilizer like PVA, which effectively prevents aggregation through steric hindrance and electrostatic repulsion. The observed nanoscale dimensions further support the potential of these clusters for applications where high surface area and fine dispersion are crucial, such as in catalysis and sensing systems. In addition, the close agreement between the DLS result and the crystallite size obtained from XRD analysis suggests that the nanoclusters are well-defined and stable in dispersion, with minimal aggregation.

3.3 AFM analysis of PVA-CuNCs

Atomic force microscopy (AFM) was employed to investigate the surface morphology and topographical features of the PVA-capped copper nanoclusters. The 3D and 2D AFM micrographs, shown in Fig. 3(a) and (b), respectively, offer a detailed view of the surface architecture at the nanoscale. The recorded particle size was approximately 6.5 nm, consistent with the ultra-small nature of the synthesized nanoclusters. The images clearly reveal that the nanoclusters exhibit an island-like surface pattern, characterized by uniformly distributed nanoscale elevations across the scanned area. This morphology is an indication of well-separated and homogeneously dispersed nanoclusters, with minimal signs of agglomeration or particle

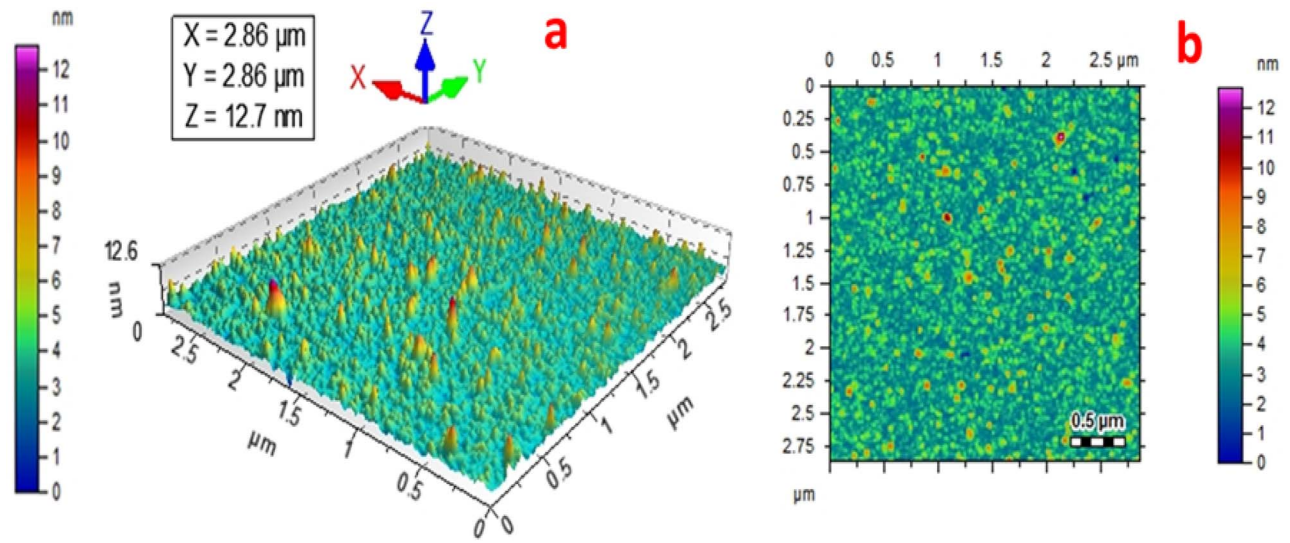

Fig. 3 (a and b) 3D and 2D AFM images of the as-prepared PVA-CuNCs, characterized by their ultra-small size and mono-disperse nature.

fusion. The topographical uniformity further validates the effectiveness of polyvinyl alcohol (PVA) as a capping and stabilizing agent, ensuring the formation of discrete CuNCs.

3.4 Electrochemical characterization of PVA-CuNCs/PtE

The electrochemical behavior of the synthesized PVA-Cu nanoclusters was investigated using cyclic voltammetry (CV) in a standard redox system consisting of 0.1 M KCl as the supporting electrolyte and 0.5 mM potassium hexacyanoferrate(III) $[Fe(CN)_6]$ as the redox probe. The measurements were conducted using both the bare platinum electrode (bare/PtE) and the PVA-CuNC-modified platinum electrode (PVA-CuNCs/PtE) to assess the enhancement in redox activity. The resulting voltammograms are displayed in Fig. 4(a). A clear difference was observed between the two electrode responses. The PVA-CuNCs/PtE electrode exhibited significantly improved redox characteristics, with a well-defined pair of oxidation and reduction peaks and enhanced peak currents compared to the bare/PtE. This significant increase in electrochemical response can be attributed to the high surface area and excellent electrical conductivity of the copper nanoclusters, which facilitate faster electron transfer kinetics between the redox species and the electrode surface. To further explore the interfacial charge transfer behavior, electrochemical impedance spectroscopy (EIS) was performed using the same electrolyte system as in the CV study, 0.1 M KCl containing 0.5 mM potassium hexacyanoferrate(III). The measurements were carried out on both the bare/PtE and the PVA-CuNCs/PtE. The resulting Nyquist plots are displayed in Fig. 4(b). A prominent difference in impedance response was observed between the two electrodes. The ohmic resistance (R_s), represented by the intercept on the real axis, was found to be approximately 6300 Ω for the bare/PtE, while it significantly decreased to about 2300 Ω for the PVA-CuNCs/PtE. This notable reduction in resistance clearly indicates improved conductivity and enhanced electron transfer at the electrode–electrolyte interface upon modification with PVA-capped copper nanoclusters. The smaller semicircular diameter in the Nyquist plot of the modified electrode reflects a lower charge transfer resistance (R_{ct}), suggesting that the nanoclusters provide a more efficient pathway for electron movement. This is attributed to the high surface area, conductive nature, and well-dispersed morphology of the CuNCs, which create a more accessible and electroactive surface for redox processes.

3.5 Electrochemical determination of anthraquinone at PVA-CuNCs/PtE

The electrochemical sensing performance of the PVA-CuNCs/PtE was examined for the detection of anthraquinone (AQ) using cyclic voltammetry (CV). The analysis was conducted in phosphate-buffered saline (PBS), with the potential window adjusted from −0.4 V to +0.8 V, and a scan rate of 220 mV s^{-1}. The CV results are displayed in Fig. 5. The PVA-CuNCs/PtE electrode exhibited a well-defined redox response in the presence of AQ, reflecting its strong electrocatalytic activity toward the quinone compound. In contrast, the bare/PtE showed a much weaker and poorly resolved redox signal under identical experimental conditions. This major difference confirms that the nanocluster modification significantly enhances the electron transfer kinetics and surface reactivity of the electrode. The superior response of PVA-CuNCs/PtE can be attributed to several factors: the ultra-small size of the CuNCs, their uniform dispersion, and the high surface-to-volume ratio, all of which provide a larger number of active sites for AQ interaction. Moreover, the PVA matrix not only stabilizes the nanoclusters but also contributes to the formation of a stable, conductive interface between the analyte and the electrode.

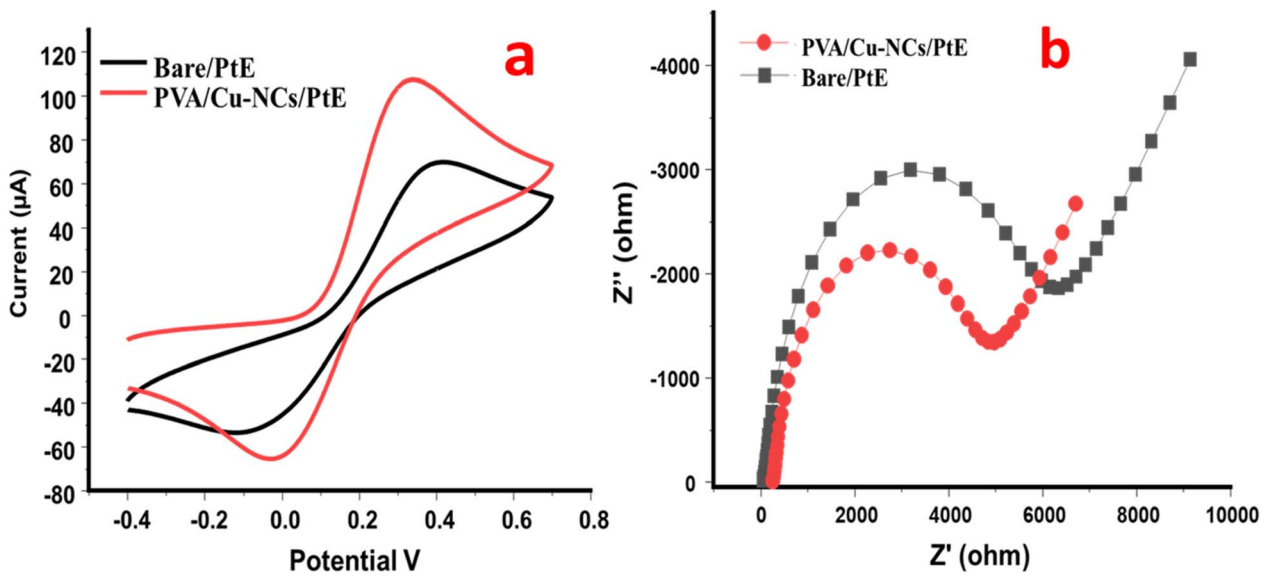

Fig. 4 (a) CV-based redox response of bare/PtE and PVA-CuNCs/PtE in 0.1 M KCl containing 0.5 mM potassium hexacyanoferrate(III) and (b) EIS Nyquist plots of bare/PtE and PVA-CuNCs/PtE.

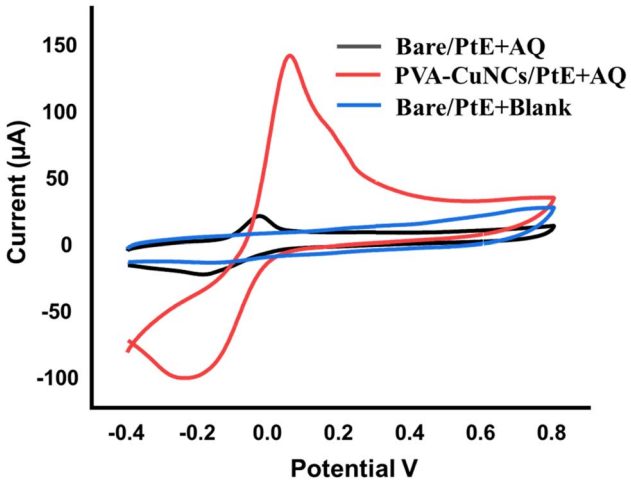

Fig. 5 CV-based redox response of AQ at PVA-CuNCs/PtE in PBS buffer at a scan rate of 220 mV s^{-1}.

3.6 Effect of electrolytes and pH study

To optimize the electrochemical environment for the detection of AQ, a comprehensive buffer study was initially performed using the PVA-CuNCs/PtE. Four different buffer systems were tested, covering a wide pH spectrum from highly acidic to basic conditions. The buffers included Britton–Robinson (BR) buffer, borate buffer, phosphate-buffer saline (PBS), and sodium hydroxide (NaOH) buffer. The comparative CV responses of AQ in different buffers are shown in Fig. 6(a). Among all tested buffers, PBS exhibited the most distinct and enhanced redox peaks, indicating a more favorable electrochemical environment for AQ oxidation and reduction. The superior response in PBS is likely due to its wide buffering capacity across the full pH range and its ability to maintain ionic strength, ensuring effective charge transfer at the electrode interface. Consequently, PBS buffer was selected as the optimal medium for further pH-dependent studies. Moreover, following buffer selection, a systematic pH study was conducted in PBS to assess the influence of proton concentration on the redox behavior of AQ. The pH was varied from acidic (pH 3) to neutral (pH 7) and basic (pH 8) conditions. The corresponding redox responses are displayed in Fig. 6(b). The results clearly indicate that the best electrochemical response was achieved at pH 6, under mild acidic conditions. At this pH, the redox peaks were sharper, and the peak current was significantly higher compared to neutral or basic environments. This suggests that proton involvement plays a key role in the redox process of AQ, and that the presence of excess H^+ ions at this pH facilitates more efficient electron transfer and reversibility.

3.7 Scan rate study

To understand the electrochemical kinetics of AQ at the surface of the PVA-CuNCs/PtE, a scan rate-dependent study was performed. The experiment was carried out in PBS at pH 6, using a fixed AQ concentration of 35 μM, while varying the scan rate from 20 to 220 mV s^{-1}. The resulting CV responses are displayed in Fig. 7(a). As the scan rate increased, the redox peak currents of AQ showed a gradual and consistent increase, reflecting the direct effect of scan rate on electron transfer dynamics. The anodic and cathodic peak currents exhibited a linear relationship with the scan rate, indicating that the redox process is likely adsorption-controlled rather than diffusion-limited under the studied conditions. This linearity is further confirmed by the corresponding calibration plots shown in Fig. 7(b), where the oxidation peak current correlated linearly with scan rate with a regression coefficient (R^2) of 0.9825, while the reduction peak current followed a similarly strong linear trend with an R^2 value of 0.9850. These high correlation coefficients confirm the reliability and stability of the electrochemical system during the scan rate sweep. The increase in peak current with higher scan rates also reflects the rapid charge transfer capability of the PVA-CuNCs/PtE interface, which efficiently facilitates the redox transitions of AQ. This behavior supports the earlier findings that the electrode surface, modified with ultra-small and

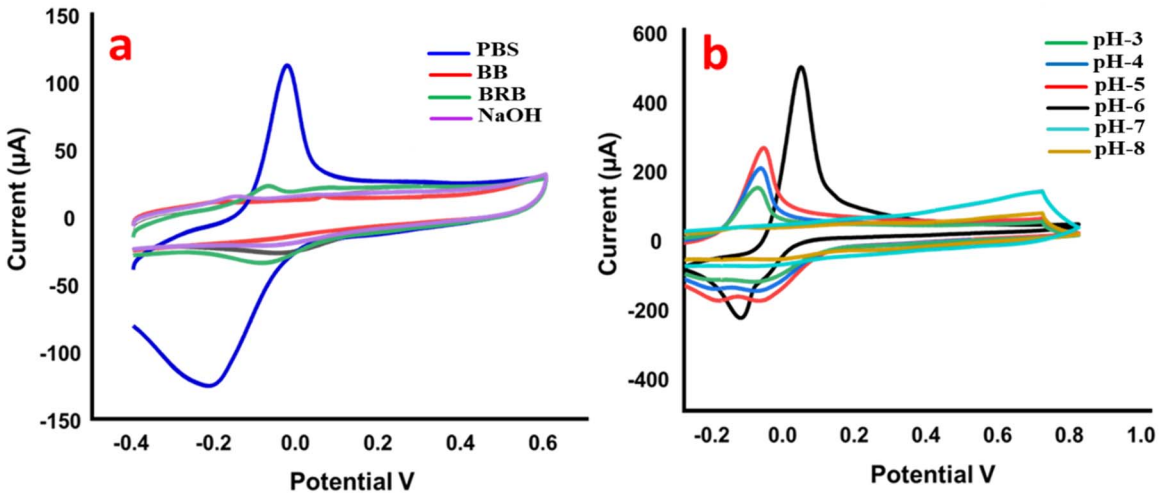

Fig. 6 (a) CV-based redox responses of AQ in different buffer systems and (b) pH-dependent CV responses of AQ at different pH levels.

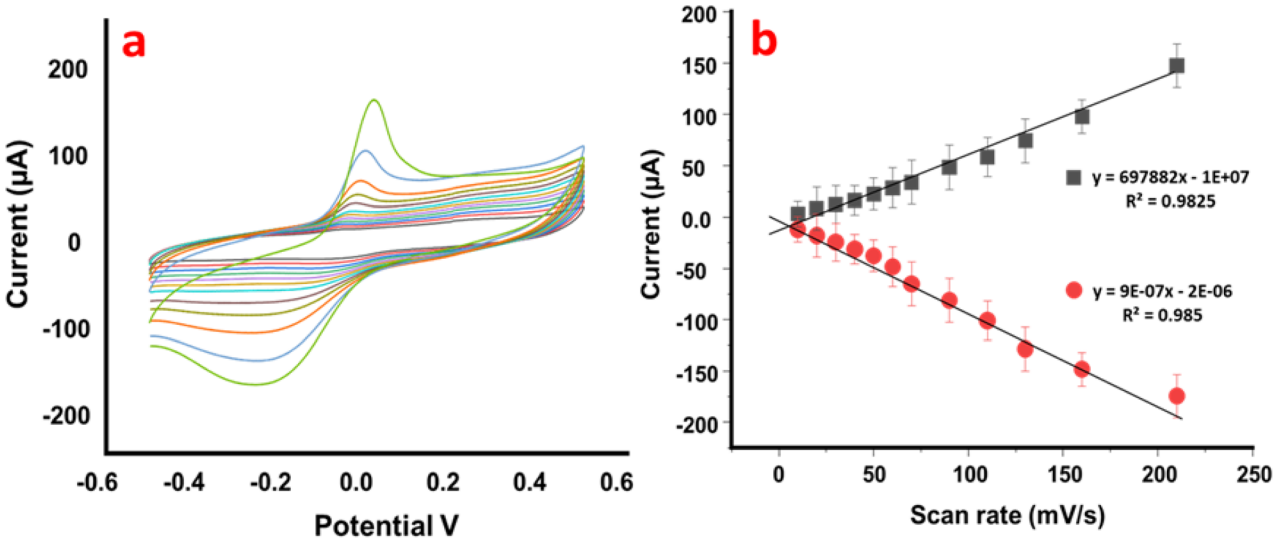

Fig. 7 (a) CV-based redox response of AQ at varied scan rates from 20 to 220 mV s^{-1} and (b) correlation coefficient for linearity in the redox response of AQ with $R^2 = 0.9825$ for the oxidation response and $R^2 = 0.9850$ for the reduction response.

homogeneously dispersed copper nanoclusters, provides a highly responsive and active platform for fast electron exchange.

Moreover, for the redox reaction of AQ at PVA-CuNCs/PtE, the AQ molecules first diffuse to the electrode surface and adsorb onto PVA-CuNCs through π–π stacking with the conjugated CuNC surface and hydrogen bonding or van der Waals interactions with the PVA functional groups.[35] The AQ molecules undergo a two-electron, two proton reduction, where they initially accept an electron from the CuNC surface to form a radical anion ($AQ^{\bullet -}$), which then rapidly gains a second electron and two protons from the PBS electrolyte to produce

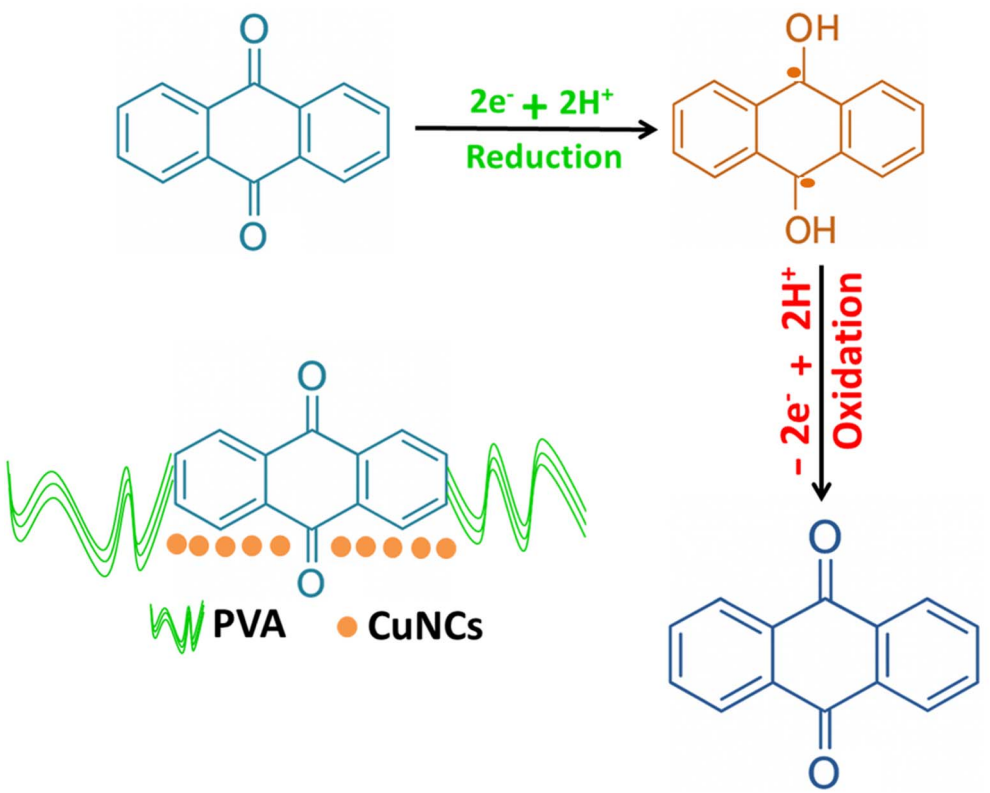

Scheme 1 Proposed redox reaction mechanism of AQ with PVA-CuNCs in PBS (pH 6) as the supporting electrolyte. AQ accepts two electrons and two protons during the reduction process to form AQH_2, which, upon reversal of potential, is oxidized back to AQ.

hydroxyanthraquinone (AQH_2). PVA-CuNCs facilitate this process by providing fast electron transfer pathways and stabilizing the radical anion *via* interaction with copper atoms. Moreover, upon reversing the potential, AQH_2 is oxidized back to AQ, completing a reversible redox cycle. The proposed redox process of the reversible reaction of AQ at PVA-CuNCs/PtE is displayed in Scheme 1. The reversibility allows repeated electrochemical measurements with consistent performance of the prepared sensor.

3.8 Repeatability and interference study

To evaluate the analytical stability and selectivity of the PVA-CuNCs/PtE for AQ sensing, both repeatability and interference tests were conducted under optimized conditions. The experiments were performed in PBS buffer at pH 6, using 30 μM AQ and a scan rate of 220 mV s^{-1}. The repeatability of the electrode response was examined by recording 30 consecutive cyclic voltammetry (CV) cycles under identical conditions. The recorded responses, shown in Fig. 8(a), demonstrate that the redox signals of AQ remained stable over multiple scans with minimal signal drift. The relative standard deviation (RSD) of the peak current was calculated as 4.37%, which falls within an acceptable range for electrochemical sensors and reflects excellent operational stability and reproducibility of the modified electrode. This result highlights the robust connection and chemical stability of the Cu nanoclusters on the electrode surface, even after repeated redox cycling. Moreover, to further investigate the selectivity of the PVA-CuNCs/PtE toward AQ, various potential interferents were introduced into the electrolyte at equimolar concentrations (30 μM). The tested interferants included structurally related redox-active compounds such as hydroquinone (HQ) and benzoquinone (BQ), common electroactive substances like ascorbic acid (AA) and hydrobromic acid (HBA), chlorinated phenols including pentachlorophenol (PCP) and trichlorophenol (TCP), as well as metal cations such as K^+, Na^+, Mg^{2+}, and Cd^{2+}. The response of AQ remained nearly unchanged in the presence of these substances, as illustrated in Fig. 8(b). No substantial deviation in peak current was observed. This result confirms that the PVA-CuNCs/PtE exhibits high selectivity for AQ detection, with strong resistance to signal interference from both organic and inorganic species.

3.9 Calibration measurement of anthraquinone

The calibration performance of the PVA-CuNCs/PtE electrode toward the detection of AQ was systematically evaluated using differential pulse voltammetry (DPV). The study was carried out in PBS at pH 6, across a wide concentration range of AQ from 0.5 μM to 220 μM. The measurements were recorded using a pulse amplitude of 220 mV s^{-1}. As depicted in Fig. 9(a), the oxidation peak current increased proportionally with rising AQ concentration, confirming a consistent and reliable electrochemical response. The linearity of the sensor was further confirmed through a calibration plot (Fig. 9(b)), which showed a strong correlation between current and concentration, yielding a regression coefficient (R^2) of 0.9808. From the calibration data, the limit of detection (LOD) and limit of quantification (LOQ) were calculated to be 0.056 μM and 0.17 μM, respectively, indicating the high sensitivity of the developed sensor system. These values reflect the excellent ability of the PVA-CuNCs/PtE to detect AQ even at trace levels, which is highly desirable in various analytical applications, including environmental monitoring. Overall, the calibration study confirms that the PVA-CuNCs/PtE sensing system is a highly reliable and sensitive platform for AQ quantification, with clear advantages over conventional electrochemical sensors. Although the prepared sensor manifested excellent response to AQ, it also faces some limitations, such as the PVA-CuNCs/PtE sensor exhibiting diminished performance at scan rates below 20 mV s^{-1}

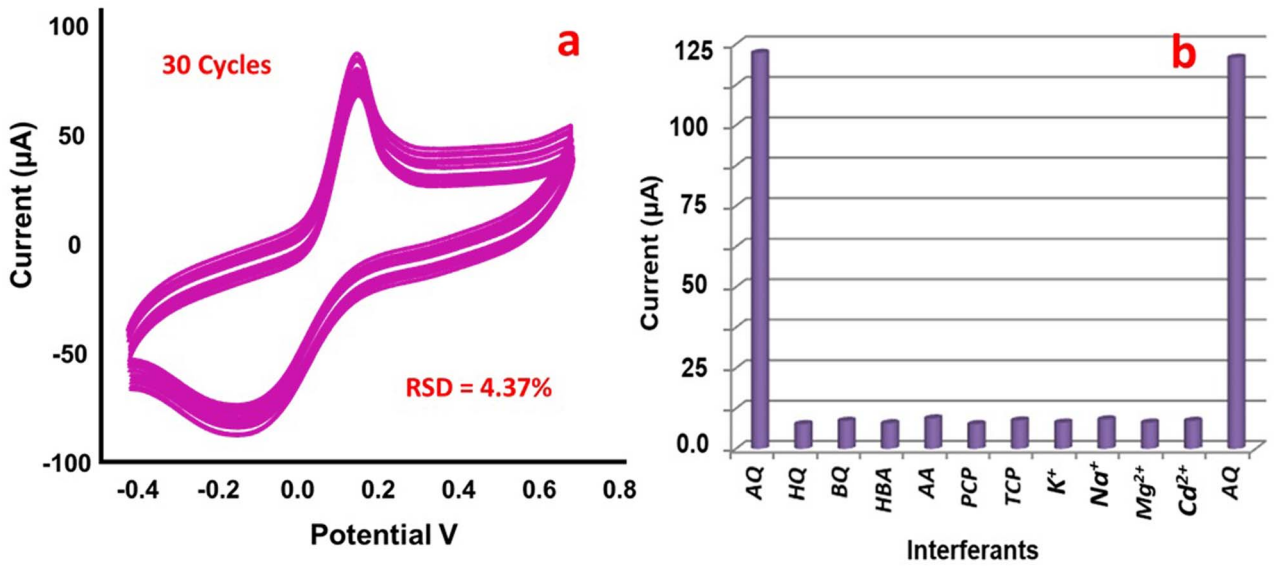

Fig. 8 (a) CV-based redox response of AQ after 30 repeated cycles at a scan rate of 220 mV s^{-1} and (b) the effect of different organic and inorganic ions on the current response of AQ.

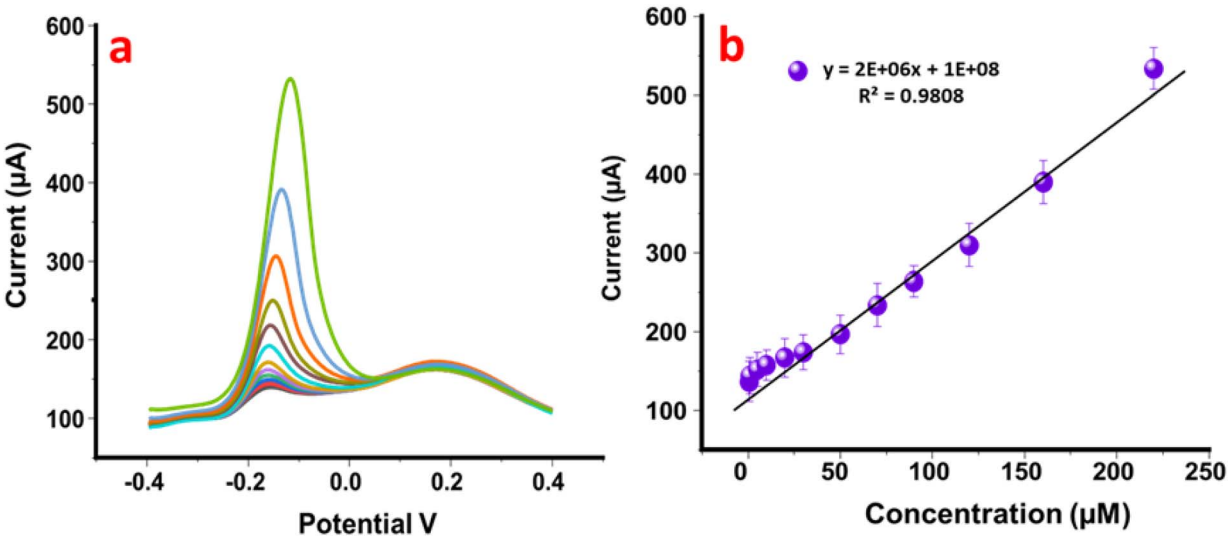

Fig. 9 (a) DPV-based oxidation peak current responses of AQ at a wide concentration range from 0.5 to 220 μM and (b) linearity of the current response with a regression coefficient of $R^2 = 0.9808$.

indicating that its response under slow scan conditions needs to be systematically explored. In addition, the long-term stability of the prepared sensor is not satisfactory, highlighting the need for further optimization to enhance durability during long-term use.

3.10 Analytical application

To assess the practical utility of the PVA-CuNCs/PtE sensor, real sample analysis was conducted for the detection of AQ, a well-known environmental pollutant. For this purpose, two different water samples were selected, one collected from the river water at Jamshoro, Sindh, Pakistan, and the other from industrial wastewater discharge from the Jamshoro Industrial Zone. These sites were intentionally chosen due to their potential exposure to organic pollutants like AQ, originating from industrial processes and urban runoff. The standard addition method was employed to evaluate AQ content in both water matrices, ensuring accuracy by compensating for potential matrix effects. A 1 : 9 ratio of phosphate buffer (pH 6) to sample was maintained for optimal electrochemical conditions.

Table 1 Real sample analysis of AQ using PVA-CuNCs/PtE as the sensing probe

Sample	Added (μM)	Detected (μM)	(%) Recovery	(%) RSD
River water	0	—	—	—
	20	19.6	98.0	4.35
	40	39.35	98.3	4.18
	60	58.95	98.2	2.96
Waste water	0	—	—	—
	20	19.84	99.2	3.39
	40	39.89	99.7	2.85
	60	59.67	99.4	4.47

The calculated recovery values ranged from 98.0% to 99.7%, with corresponding relative standard deviation (RSD) values within acceptable analytical limits, indicating excellent precision and repeatability. The complete recovery data are summarized in Table 1. These results demonstrate that the PVA-CuNCs/PtE sensing system provides accurate detection of AQ in real environmental samples, supporting its viability as a reliable tool for monitoring pollutant levels in complex aqueous environments.

4 Conclusion

In conclusion, the development of PVA-capped Cu nanoclusters *via* a simple chemical reduction method has proven effective for fabricating a stable and highly functional electrochemical sensing platform. The detailed physicochemical characterization validated the crystalline purity, nanoscale size, and well-dispersed morphology of the synthesized PVA-CuNCs. These structural and surface properties directly contributed to the enhanced electrochemical behavior observed in the detection of AQ. The PVA-CuNCs/PtE electrode exhibited a strong and stable redox response under optimized conditions in phosphate-buffered saline (PBS) at pH 6, with a low detection limit of 0.056 μM, demonstrating its high sensitivity. Furthermore, the sensor was successfully applied to different environmental samples, including river and industrial water samples, where it demonstrated accurate quantification with recovery rates ranging from 98.0% to 99.7%. These findings clearly establish the reliability and environmental relevance of the proposed sensor. The combination of a simple synthesis route, thorough material characterization, and excellent analytical performance positions this method as a promising candidate for future applications in pollutant monitoring and real-time electrochemical sensing. Although the prepared sensor manifested excellent response to AQ, it also faces some limitations, such as

the PVA-CuNCs/PtE sensor exhibiting diminished performance at scan rate below 20 mV s^{-1}, indicating that its response under slow scan conditions needs to be systematically explored. In addition, the long-term stability of the prepared sensor is not satisfactory, highlighting the need for further optimization to enhance durability during long-term use.

In addition, the future perspective of this work should aim to optimize the electrode design to improve stability and sensitivity. Exploring the sensor's performance in complex real sample matrices will further validate its practical applicability. Integration with miniaturized or portable devices could enable on-site point-of-care monitoring. Moreover, expanding its application to detect a wide range of environmental pollutants and biomedical targets will broaden its utility and impact.

Author contributions

All authors have equal contribution in writing, formatting, editing, sampling, characterization, analysis and electrochemical detection process.

Conflicts of interest

All authors declare that they have no competing interests.

Data availability

The data will be made available upon request.

References

1 I. O. Minatel, C. V. Borges, M. I. Ferreira, H. A. G. Gomez, C.-Y. O. Chen and G. P. P. Lima, *Phenolic Compd.:Biol. Act.*, 2017, **8**, 1–24.
2 M. Shahid, J. Wertz, I. Degano, M. Aceto, M. I. Khan and A. Quye, *Anal. Chim. Acta*, 2019, **1083**, 58–87.
3 A. K. Tolkou, A. C. Mitropoulos and G. Z. Kyzas, *Environ. Sci. Pollut. Res.*, 2023, **30**, 73688–73701.
4 L. A. Goulart and L. H. Mascaro, *Electrochim. Acta*, 2016, **196**, 48–55.
5 Y. Zheng, M. Ma, X. Zou, X. Yin, J. Zhu and C. Chen, *J. Environ. Chem. Eng.*, 2024, **12**, 114489.
6 P. Liu, H. Zhang, Y. Chen, Y. Di, Z. Li, B. Zhu, Z. Liu, Z. Zhang and F. Wang, *RSC Sustainability*, 2024, **2**, 483–490.
7 X. Yang, C. He, W. Lin, Y. Qiu, P. Li, Y. Chen, B. Huang and X. Zheng, *Synth. Met.*, 2022, **287**, 117079.
8 A. C. d. Sá, S. C. Barbosa, P. A. Raymundo-Pereira, D. Wilson, F. M. Shimizu, M. Raposo and O. N. Oliveira Jr, *Chemosensors*, 2020, **8**, 103.
9 Y. Xue, M. Noroozifar, R. M. A. Sullan and K. Kerman, *Chemosphere*, 2023, **342**, 140003.
10 H. Meskher and F. Achi, *Crit. Rev. Anal. Chem.*, 2024, **54**, 1354–1367.
11 T. C. Canevari, P. A. Raymundo-Pereira, R. Landers and S. A. Machado, *Eur. J. Inorg. Chem.*, 2013, **2013**, 5746–5754.
12 S. Hu, W. Zhang, J. Zheng, J. Shi, Z. Lin, L. Zhong, G. Cai, C. Wei, H. Zhang and A. Hao, *RSC Adv.*, 2015, **5**, 18615–18621.
13 Y. Li, P. Cao, S. Wang and X. Xu, *Bioresour. Technol.*, 2022, **347**, 126691.
14 H. Wang, Q. Li, N. He, Y. Wang, D. Sun, W. Shao, K. Yang and Y. Lu, *Sep. Purif. Technol.*, 2009, **67**, 180–186.
15 N. Liu and G. Sun, *Ind. Eng. Chem. Res.*, 2011, **50**, 5326–5333.
16 J. A. Buledi, A. R. Solangi, A. Hyder and A. Mallah, in *Functionalized Magnetic Nanohybrids*, ed. K. Rizwan and A. Baykal, Elsevier, 2025, pp. 415–434.
17 A. Hyder, M.-U.-N. Khilji, J. A. Buledi, A. A. Memon, A. Ghanghro, M. ur Rehman and K. H. Thebo, *RSC Sustainability*, 2025, **3**, 2160–2184.
18 A. Hyder, A. Ali, J. A. Buledi, R. Memon, B. S. Al-Anzi, A. A. Memon, M. Kazi, A. R. Solangi, J. Yang and K. H. Thebo, *Phys. Chem. Chem. Phys.*, 2024, **26**, 10940–10950.
19 J. A. Buledi, A. R. Solangi, A. Hyder, N. H. Khand, S. A. Memon, A. Mallah, N. Mahar, E. N. Dragoi, P. Show, M. Behzadpour and H. Karimi-Maleh, *Food Chem. Toxicol.*, 2022, **165**, 113177.
20 A. Hyder, S. S. Memon, J. A. Buledi, S. Memon, Z.-u.-A. Memon, S. G. Shaikh and D. B. Rajpar, *Chem. Pap.*, 2023, **77**, 7737–7748.
21 D. Sahu, P. Mohapatra and S. K. Swain, *J. Photochem. Photobiol., A*, 2020, **386**, 112098.
22 X. Liu and D. Astruc, *Coord. Chem. Rev.*, 2018, **359**, 112–126.
23 Z. Wang, B. Chen and A. L. Rogach, *Nanoscale Horiz.*, 2017, **2**, 135–146.
24 A. Hyder, J. A. Buledi, M. Nawaz, D. B. Rajpar, Z.-u.-H. Shah, Y. Orooji, M. L. Yola, H. Karimi-Maleh, H. Lin and A. R. Solangi, *Environ. Res.*, 2022, **205**, 112475.
25 N. Wang, L. Ga, M. Jia and J. Ai, *J. Nanomater.*, 2019, 2019.
26 A. Henglein, *Chem. Phys. Lett.*, 1989, **154**, 473–476.
27 L.-Y. Chen, C.-W. Wang, Z. Yuan and H.-T. Chang, *Anal. Chem.*, 2015, **87**, 216–229.
28 K. Okitsu, M. Ashokkumar and F. Grieser, *J. Phys. Chem. B*, 2005, **109**, 20673–20675.
29 C. Wang, C. Wang, L. Xu, H. Cheng, Q. Lin and C. Zhang, *Nanoscale*, 2014, **6**, 1775–1781.
30 Y.-S. Borghei, M. Hosseini and M. R. Ganjali, *Microchim. Acta*, 2017, **184**, 2671–2677.
31 N. Su, X. Gao, X. Chen, B. Yue and H. He, *J. Catal.*, 2018, **367**, 244–251.
32 D. P. Stankus, S. E. Lohse, J. E. Hutchison and J. A. Nason, *Environ. Sci. Technol.*, 2011, **45**, 3238–3244.
33 A. Hyder, S. Sanam Memon, S. Memon, S. Sirajuddin, Z.-u.-A. Memon, D. Bux Rajpar, S. Gul Shaikh and J. Ahmed Buledi, *Microchem. J.*, 2021, **163**, 105908.
34 A. Hyder, J. A. Buledi, R. Memon, A. Qureshi, J. H. Niazi, A. R. Solangi, S. Memon, A. A. Memon and K. H. Thebo, *Diamond Relat. Mater.*, 2023, **139**, 110357.
35 P. S. Guin, S. Das and P. C. Mandal, *Int. J. Electrochem.*, 2011, 816202.